Check for updates

f-Block reactions of metal cations with carbon dioxide studied by inductively coupled plasma tandem mass spectrometry

Richard M Cox, [ID] * Kali M. Melby, [ID] Amanda D. French [ID] and Michael J. Rodriguez [ID]

f-Block chemistry offers an opportunity to test current knowledge of chemical reactivity. The energy dependence of lanthanide cation ($Ln^+ = Ce^+, Pr^+, Nd^+-Eu^+$) and actinide cation ($An^+ = Th^+, U^+-Am^+$) oxidation reactions by CO_2, was observed by inductively coupled plasma tandem mass spectrometry. This reaction is commonly spin-unallowed because the neutral reactant (CO_2, $^1\Sigma_g^+$) and product (CO, $^1\Sigma^+$) require the metal and metal oxide cations to have the same spin state. Correlation of the promotion energy (E_p) to the first state with two free d-electrons with the reaction efficiency indicates that spin conservation is not a primary factor in the reaction rate. The E_p likely influences the reaction rate by partially setting the crossing between the ground and reactive states. Comparison of Ln^+ and An^+ congener reactivity indicates that the 5f-orbitals play a small role in the An^+ reactions.

Introduction

The f-block, or elements with f-electrons in the valence shells, represents an interesting frontier in chemistry. While understanding f-block chemistry is vital for the nuclear industry to ensure safe and efficient operation, the f-block represents an opportunity to confirm or revise our current understanding of chemical reactions because most of our understanding of chemical theory is derived from work with s, p, and d-blocks. The radial distribution of the 4f-orbitals suggests that their participation in bonding will be minimal, but the 5f-orbitals have the correct distribution to participate. Nevertheless, the parameters of when the 5f-orbitals participate in bonding are unclear.

While many current studies focus on condensed phases, gas phase studies offer an attractive alternative. Gas phase studies eliminate many perturbations in condensed phases like solvent effects so that the fundamental interaction of the analyte species can be probed. Indeed, mass spectrometry has proven adept at observing the reactions of actinides (An) and lanthanides (Ln). Fourier transform ion cyclotron resonance mass spectrometry (FTICR-MS) has been utilized to study An^+ ($An^+ = Th^+-Cm^+$) with many small molecules.[1–6] Similar reactions of the Ln^+ with small molecules have been studied using selected ion flow tube mass spectrometry (SIFT-MS).[7–9] Unfortunately, FTICR-MS and SIFT-MS are thermal methods where only

barrierless, exothermic or thermoneutral reactions can be observed, somewhat limiting the impact of the studies and the reactions that can be probed. Furthermore, observation of a reaction at a single energy point can mislead conclusions. For example, the low efficiency reaction observed between $Th^+ + CH_4$ in FTICR-MS experiments was originally attributed to spin-restrictions;[4] however, it was shown later in energy dependence studies by guided ion beam tandem mass spectrometry (GIBMS) to be caused by a small barrier[10] where the low efficiency reaction was observed from a small population of reactants within the energy distribution with sufficient energy to overcome the reaction barrier.

GIBMS[10–27] oxidation studies shed light on the reaction by observing it over a wide range of kinetic energies. The energy dependence of the reaction often simplifies the interpretation of results, as noted in the GIBMS study of $Th^+ + CH_4$,[10] and allows the observation of endothermic reactions or reactions with a barrier. However, many of the An elements are significantly radioactive so that they are difficult to obtain and work with safely. Consequently, studies of the energy dependence of transuranic species have not been reported in the gas phase. Yet there remain examples of low efficiency reactions, for example $Pu^+ + CO_2$ from FTICR-MS studies,[1] that may require knowing the energy dependence of the reaction to correctly interpret.

Additionally, the reactions of Ln^+ and An^+ with CO_2 is an interesting system to study, in part because SIFT-MS[7] and FTICR-MS[1,2] studies provide examples of exothermic reactions where no or limited product is observed. Furthermore, atmospheric CO_2 also remains a large reservoir of carbon that can

Pacific Northwest National Laboratory, Richland, WA 99352 USA, USA.
E-mail: richard.cox@pnnl.gov

This journal is © the Owner Societies 2024

*Phys. Chem. Chem. Phys.*, 2024, **26**, 209–218 | **209**

potentially be tapped with the correct catalyst. However, CO_2 is difficult to crack because activating the C=O bond according to reaction (1) is formally spin-forbidden:

$$CO_2(^1\Sigma_g^+) \rightarrow CO(^1\Sigma^+) + O(^3P) \qquad (1)$$
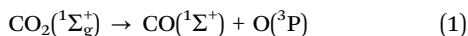
The spin allowed pathway lies 1.97 eV higher in energy dissociating to the CO + O (^{1}D).[28] Nevertheless, developing an economical catalyst that can break the C=O bond could revolutionize manufacturing and lead to a promising method to remove excess carbon from the atmosphere. While transuranics are unlikely to be that catalyst, they offer an extreme system to test chemical theory upon.

For CO_2, reaction (2) is often spin-forbidden because unpaired electrons in the metal cation (M^+) and oxygen usually pair when forming MO^+ to lower the spin in the metal oxide cation product:

$$M^+(^sL) + CO_2(^1\Sigma^+) \rightarrow MO^+(^{s-2}\Lambda) + CO(^1\Sigma^+) \qquad (2)$$
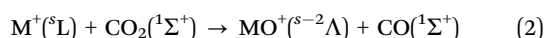
where s is the spin-multiplicity. This spin-restriction is often cited as a reason that reactions proceed inefficiently.[1,4] However, it is unclear why spin-conservation should apply to large metals. Indeed, recent work by Cox *et al.*,[22] which analyzed the observed efficiency of Ln^+ and An^+ cations reactions with O_2, CO_2 and H_2O at thermal energies,[1–3,5,7–9] concluded that the primary influence on the reaction rate was the promotion energy (E_p) from the ground state to the first state with two free nd-electrons, where n = 5, 6. This correlation appears to be caused because the free nd-electrons are necessary to form an efficient LnO^+ or AnO^+ bond; therefore, the rate is at least partially influenced by the crossing between the potential energy surfaces evolving from the ground state and the more reactive higher energy state at $E_p(nd^2)$.

Here we present the energy dependence of An^+ (An^+ = Th^+, U^+–Am^+) reactions with CO_2 studied using an Agilent 8900 inductively coupled plasma tandem mass spectrometry (ICP-MS/MS) over an extended energy range. The goal of this study is to understand the role of the An^+ valence electrons, and specifically the 5f-orbitals, in the reaction through observing the reactivity trend across the An series. For comparison as a baseline when f-electrons are not expected to contribute,[29,30] the energy dependence of Ln^+ (Ln^+ = Ce^+, Pr^+, Nd^+, Sm^+, Eu^+) reactions are also presented.

Experimental methods

Caution: The An used in this study are all radioisotopes with varying activities and half-lives. All work was done within the radiological protection controls of specialized laboratories at Pacific Northwest National Laboratory.

Experiments were conducted using an Agilent 8900 "triple quadrupole" mass spectrometer (ICP-MS/MS; Agilent Technologies, Santa Clara, CA, USA) located within a radiological facility at Pacific Northwest National Laboratory.[31] This instrument utilized an ICP ion source equipped with a quartz double-pass spray chamber and 100 μL min^{-1} perflouroalkoxy alkane (PFA) nebulizer. The instrument utilizes a quadrupole mass filter (1 amu resolution) to mass

Table 1 Average electronic energy (in eV) of Ln^+ and An^+ from the ICP source assuming a Boltzmann distribution[a]

M^+ (isotope)	Mass (amu)	300 K	700 K	5000 K	8000 K	9000 K	10 000 K
Ce^+ (140)	139.90	0.00	0.04	0.58	0.69	0.71	0.74
Pr^+ (141)	140.91	0.01	0.03	0.42	0.54	0.57	0.61
Nd^+ (146)	145.91	0.01	0.03	0.57	0.79	0.85	0.90
Sm^+ (149)	148.92	0.02	0.06	0.43	0.59	0.64	0.69
Eu^+ (153)	152.92	0.00	0.01	0.28	0.68	0.81	0.93
Th^+ (232)	232.04	0.00	0.02	0.66	0.85	0.90	0.93
U^+ (238)	238.05	0.01	0.03	0.51	0.67	0.71	0.74
Np^+ (237)	237.05	0.00	0.01	0.23	0.28	0.30	0.31
Pu^+ (242)	242.06	0.00	0.01	0.70	0.87	0.91	0.95
Am^+ (243)	243.06	0.00	0.00	0.19	0.52	0.63	0.75

[a] Masses and electronic states taken from ref. 28 (https://physics.nist.gov/PhysRefData/Handbook/periodictable.htm).

select the reactant ion beam that is passed into a collision cell contained within an octopole ion guide where the reactant ion is reacted with the neutral gas, CO_2. Products and unreacted ions drift to the end of the octopole where they are focused through a second quadrupole mass filter, mass selected, and subsequently detected at a standard electron multiplier detector.

Stock multi-element standard solutions containing 1 ng g^{-1} of Ce–Nd, Sm, Eu, Th, and U in 2% HNO_3 were prepared. To minimize high activity radioisotopes within the instrument, a multi-element standard solution of 1 pg g^{-1} of Np–Am in 2% HNO_3 was also prepared. Table 1 lists the isotopes used for each M^+. Carbon dioxide (CO_2; 99.99%; Oxarc) was used as the reaction gas. The flow rates ranged from 0.06–0.13 mL min^{-1}, which corresponds to estimated pressures of 1.4 and 2.8 mTorr. Tuning parameters were optimized to provide maximum sensitivity for the high mass range using a 1 ng g^{-1} Th and U solution. The octopole bias was adjusted in intervals from +7 V to −45 V while keeping other cell parameters constant: octopole rf peak-to-peak voltage of 180 V, axial acceleration of 2.0 V, and a kinetic energy discrimination (KED, the voltage difference between the octopole bias in the CRC and the second quadrupole) of −10.0 V. Data were acquired in triplicate using 1 s acquisition times for the 1 ng g^{-1} solutions and 4 s for the 1 pg g^{-1} solutions.

Kinetic energy dependent cross section

Reaction cross sections (σ) are calculated from the raw signal intensities using a Beer's Law analog:[32]

$$I = I_0 e^{-\rho \sigma l} \qquad (3)$$

where I is the reactant intensity exiting the collision cell, I_0 is the reactant intensity entering the collision cell, ρ is the number density of the neutral reactant in the collision cell, and l is the effective length of the collision cell. I_0 is estimated from the sum of all ion signals observed after the second quadrupole from the mass selected in the first quadrupole. l is estimated as the physical length of the collision cell, 10 cm, in the Agilent 8900. This is not strictly correct because a pressure gradient will exist at the entrance and exit apertures that will lengthen the effective cross section. The difference is anticipated to be ≤20% and is incorporated into the absolute uncertainty of the cross section. Individual product cross sections (*e.g.*, MO^+) are calculated as a

210 | *Phys. Chem. Chem. Phys.*, 2024, **26**, 209–218

This journal is © the Owner Societies 2024

percentage of the overall reaction cross section; however, only MO^+ or MO_2^+ products were observed. Because the Agilent 8900 operates under multi-collision conditions, to compare the observed cross section to the reaction collision limit, the cross sections observed at 1.4 and 2.8 mTorr were extrapolated to zero pressure for rigorous single collision conditions. Absolute uncertainties in the cross section are estimated to be $\pm 50\%$ with relative uncertainties of $\pm 10\%$.

The energy in the laboratory frame is estimated from the octopole bias by the relationship:[33]

$$E_{Lab} = V_p + \frac{m}{m_{Ar}}\frac{5}{2}k_B T_P - V_{oct} \qquad (4)$$

where V_p is the plasma potential (~ 2 V), m is the reactant ion, M^+, mass, m_{Ar} is the mass of argon, k_b is Boltzmann's constant, T_p is the ion temperature entering the octopole, and V_{oct} is the octopole bias. The temperature of the ion exiting the plasma is expected to be the plasma temperature, 8000–10 000 K. Collisional cooling in a differential pumping region between the source and first quadrupole is expected to drop the average temperature entering the octopole, so T_p is conservatively estimated to be 5000–10 000 K. Table 1 lists the average electronic energy for a Boltzmann distribution in these temperature ranges. Above 5000 K, average electronic energy can be significant, and this difference likely affects the reactivity observed where excited states may be more or less reactive than the ground state. Because of the great number of overlapping electronic states, it is assumed that a pathway exists from any given excited state to the lowest energy reaction surface leading to products. Consequently, the average electronic energy is treated as energy available for reaction. The energy in the center-of-mass (E_{CM}) frame represents the kinetic energy available for a chemical reaction. The relationship between E_{LAB} and E_{CM} is described by eqn (5):[32]

$$E_{CM} = E_{LAB} \times M/(M + m) \qquad (5)$$

where M is the mass of the neutral reactant partner, CO_2 = 44.01 amu and m is the mass of the metal ion.

Calculating reaction efficiency

Reaction efficiency is calculated relative to the collision limit (k_c). The collision limit is estimated using the Langevin–Gioumousis–Stevenson (LGS) model[34] with a polarizability of 2.59×10^{-24} cm^3 for CO_2.[35] Two approaches were taken to calculating the reaction efficiency. The first approach was to calculate the efficiency at the lowest observed energy (E_{CM}) observed, 0.15–0.3 eV. This is similar to single energy methods, SIFT-MS or FTICR-MS, calculations, although the corresponding temperatures here are 1600–2300 K. The second approach was to average the calculated efficiencies for all results below 1 eV. Deviations in the cross section reaction energy dependence have been observed for the Th^+ reaction with O_2 in GIBMS experiments.[13] Nevertheless, no deviations above 10% of the mean efficiency were observed calculating the efficiency in this manner with the exception to Sm^+ and Pu^+, where the cross sections suggest a weak barrier in excess of the reaction enthalpy. The minimum efficiency reported was k/k_{col} = 0.01.

Experimental results

$Ln^+ + CO_2$

The absolute cross section as a function of kinetic energy for reaction (2) (M^+ = Ce^+, Pr^+, Nd^+, Sm^+, Eu^+) are presented in Fig. 1. Only two products, MO^+ and MO_2^+, were observed, although MC^+ and MCO^+ were explicitly looked for and not observed. Of these products, MO_2^+ had a clear dependence on CO_2 pressure suggesting that it is formed through the secondary reaction, reaction (6):

$$MO^+ + CO_2 \rightarrow MO_2^+ + CO \qquad (6)$$
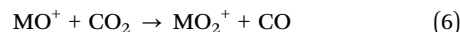
A minor pressure dependence was also observed for reaction (2), likely associated with MO^+ depletion from reaction (6). The cross sections shown in Fig. 1 has been extrapolated to zero pressure to remove all dependencies from the CO_2 pressure.

The cross sections of CeO^+, PrO^+, and NdO^+ formed in reaction (2) initially decrease with increasing energy consistent with a barrierless exothermic reaction until energies near 2.4, 1.9, and 1.2 eV, respectively. Beyond the initial decline, the cross sections increase peaking near the OC=O bond dissociation energy, $D_0(OC-O)$ = 5.453 eV[36] where sufficient energy is available for MO^+ to dissociate. It should be noted that the initial low energy feature obscures where this increase begins making it likely that the more efficient the reaction, the more likely the threshold of the higher energy feature is obscured. Conversely, the cross sections of SmO^+ and EuO^+ increase with increasing energy. For SmO^+, where $D_0(Sm^+-O)$ = 5.596 $\pm$ 0.004 eV,[37] the observed cross section indicates a barrier to this reaction, which is exothermic by 0.143 eV. This behavior has been observed previously in GIBMS experiments.[15] In the present experiment, the apparent threshold is shifted to lower energies than that
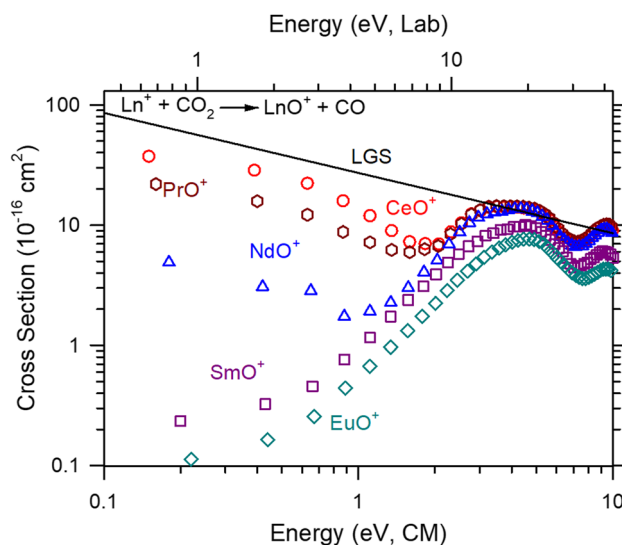
Fig. 1 Reaction cross section of Ln^+ [Ln^+ = Ce^+ (red circles), Pr^+ (dark red octagons), Nd^+ (blue triangles), Sm^+ (purple squares), Eu^+ (teal diamonds)] + $CO_2 \rightarrow LnO^+ + CO$ as a function of kinetic energy in CM frame (lower x-axis). The black line represents the Langevin–Gioumousis–Stevenson (LGS) model cross section. E_{Lab} of $^{146}Nd^+$ is represented on the upper x-axis.

observed in the GIBMS experiment, indicating the presence of excited states. Given the typical operating temperature of the ICP plasma is 8000–10 000 K, the observation of excited states from this source is expected. A second increase in cross section magnitude is also observed for all Ln^+ peaking around 10 eV. This may be an effect from ion focusing caused by the interaction between differing radio frequencies between the two quadrupoles and octopole regions within the instrument No effort is made to interpret or characterize this feature.

The reaction efficiencies (k/k_{col}) of the Ln^+ reactions relative to the Langevin–Gioumousis–Stevenson (LGS) collision limit[34] (k_{col}) are listed in Table 2. Two approaches were taken to calculate the reaction efficiency. The first approach was to average the k/k_{col} for all energies below 1 eV. The second approach was to calculate the k/k_{col} for the lowest observed energy, 0.15–0.2 eV, which corresponds to measuring the reaction efficiency at $\approx$1600–2300 K. For the Ln^+, the difference between each approach is minimal. For comparison, the reaction efficiencies of GIBMS,[15,17,19] selected ion flow tube mass spectrometry (SIFT-MS),[7] and FTICR-MS[38] efficiencies are also listed in Table 2. In general, the ICP-MS/MS values here are within the combined uncertainties of the previous measurements. The largest observed difference was for Pr^+ where the GIBMS and SIFT-MS value are half of the ICP-MS/MS mean (but still within the combined measurement uncertainty). This difference can likely be attributed to the difference in the metal cation electronic distribution. Smaller differences for the other Ln^+ can also be attributed to electronic distributions.

An$^+$ + CO$_2$

Absolute cross sections as a function of kinetic energy for reaction (2) (M^+ = Th^+, U^+–Am^+) are presented in Fig. 2. Like the Ln^+, only MO^+ and MO_2^+ products were observed. After extrapolating to zero pressure, only MO^+ was observed. ThO^+, UO^+, and NpO^+ cross sections decrease with increasing energy consistent with a barrierless exothermic reaction. After the initial decline in the cross sections, like the Ln^+, an increase in the cross section is observed $\approx$2.0, 1.9, and 1.3 eV,
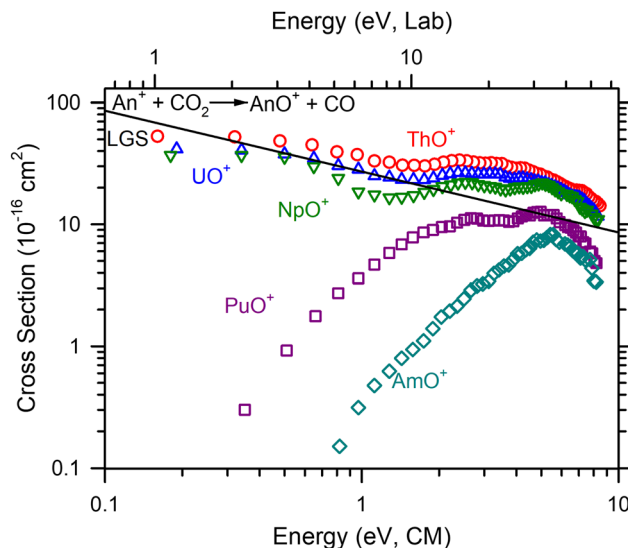

Fig. 2 The reaction cross sections of An$^+$ [An$^+$ = Th$^+$ (red circles), U$^+$ (blue triangles), Np$^+$ (green inverted triangles), Pu$^+$ (purple squares), Am$^+$ (teal diamonds)] + CO$_2$ → AnO$^+$ + CO as a function of kinetic energy in the CM frame (lower x-axis). The black line represents the Langevin–Gioumousis–Stevenson (LGS) model cross section. E_{Lab} of $^{238}U^+$ is represented on the upper x-axis.

respectively. However, for the An$^+$, this feature is much less pronounced than observed in the Ln^+. This may be because the An$^+$ reactions are more efficient obscuring the magnitude of the second energy feature. Curiously, PuO^+ and AmO^+ have increasing cross sections with increasing energy. Given $D_0(Pu^+–O)$ = 6.75 $\pm$ 0.20 eV, $D_0(Am^+–O)$ = 5.80 $\pm$ 0.29 eV[39] and $D_0(OC–O)$ = 5.45 eV,[36] these cross sections indicate a clear barrier in excess of the reaction enthalpy.

A comparison of k/k_{col} between the two methods indicates that the average efficiency below 1 eV differs from the efficiency determined from the lowest energy point. This difference largely disappears when comparing the second energy point to the average. Previous measurements of reaction efficiency (Table 2), are primarily limited to FTICR-MS measurements by Gibson and coworkers.[1,2] Additional measurements for Th$^+$ and

Table 2 Comparison of rection efficiencies (k/k_{col}) for M$^+$ + CO$_2$ → MO$^+$ + CO^a

M$^+$	$E_p(nd^2)^b$	This work^c	This work^d	GIBMS	SIFT-MS^e	FTICR-MS
Ce$^+$	0.00	0.86 $\pm$ 0.43	0.77 $\pm$ 0.38	0.48 $\pm$ 0.10^f	0.66 $\pm$ 0.20	0.70 $\pm$ 0.25^g
Pr$^+$	0.73	0.50 $\pm$ 0.25	0.47 $\pm$ 0.23	0.25 $\pm$ 0.05^h	0.23 $\pm$ 0.07	
Nd$^+$	1.14	0.12 $\pm$ 0.06	0.12 $\pm$ 0.06	0.09 $\pm$ 0.02^i	0.05 $\pm$ 0.02	0.08 $\pm$ 0.03^g
Sm$^+$	2.35	0.01 $\pm$ 0.01	NR^j	NR^{jk}	NR^j	
Eu$^+$	3.74	NR^j	NR^j		NR^j	
Th$^+$	0.00	1.19$\pm$ 0.60	0.79 $\pm$ 0.40	0.88 $\pm$ 0.18^b		0.95 $\pm$ 0.33^g
						0.35 $\pm$ 0.18^l
U$^+$	0.57	0.93 $\pm$ 0.47	0.66 $\pm$ 0.33	>1^m, 1.18 $\pm$ 0.24^n		1.02 $\pm$ 0.36^g
						0.29 $\pm$ 0.15^l
Np$^+$	0.9 $\pm$ 0.4	0.77 $\pm$ 0.39	0.58 $\pm$ 0.29			0.30 $\pm$ 0.15^l
Pu$^+$	2.14	0.05 $\pm$ 0.03	NR^j			0.003 $\pm$ 0.002^l
Am$^+$	3.6 $\pm$ 0.2	NR^j	NR^j			0.001 $\pm$ 0.001^o

^{a} k_{col} is derived from the Langevin–Gioumosis-Stevenson model cross section for CO$_2$. ^{b} See ref. 22 and references therein. ^{c} Average k/k_{col} for all energies <1 eV. ^{d} k/k_{col} for the lowest energy measured (0.15–0.20 eV). ^{e} Ref. 7. ^{f} Work in progress, see ref. 26. ^{g} Ref. 38. ^{h} Ref. 19. ^{i} Ref. 17. ^{j} No reaction observed. ^{k} A barrier in excess of the thermodynamic threshold was observed. See ref. 15. ^{l} Ref. 1. ^{m} Ref. 11. ^{n} Work in progress, see ref. 25. ^{o} Ref. 2.

212 | *Phys. Chem. Chem. Phys.*, 2024, **26**, 209–218

This journal is © the Owner Societies 2024

U^+ are available from FTICR-MS,[38] GIBMS (Th^+),[22] and an early ion beam experiment (U^+).[11] The Th^+ and U^+ efficiencies reported here compare well with the ion beam[11,22] and FTICR-MS results from Cornehl *et al.*[38] The FTICR-MS measurements of Gibson and coworkers[1,2] are lower than those observed here with the exception of Pu^+ and Am^+ where very inefficient reactions under nominally thermal conditions were observed in the FTICR-MS work. Note that the FTICR-MS measurements of Gibson and coworkers[1,5] are systematically lower than those observed in GIBMS experiments as observed for several reactions with Th^+,[13,18,22,40] U^+,[23] and Gd^+.[14,16] The differences in k/k_{col} between measurements has been previously attributed to a different starting ion electronic energy distribution.[10,13]

Comparison to GIBMS cross sections

GIBMS cross sections for reaction (2) have been reported for Pr^+,[19] Nd^+,[17] Sm^+,[15] and Th^+[22] by Armentrout and coworkers. Early ion beam cross sections have also been published for U^+ by Armentrout and Beauchamp.[11] As noted above, the efficiency for the Ln^+ species reported here, generally exceeds the efficiency reported in the GIBMS experiments. This could be caused by the use of higher energies in the calculation of reaction efficiency than are typically used in the GIBMS experiments (*e.g.* k/k_{col} for Pr^+ is calculated at 0.05 eV).[19] However, a direct comparison of cross sections indicate some differences in absolute magnitude. In the case of Th^+, the absolute magnitude at the cross section peak centered at ≈ 5.5 eV is +50% for the ICP-MS/MS cross section compared to the GIBMS cross section.[22] This is similar to the difference in the peak magnitude between ICP-MS/MS and GIBMS for Nd^+.[17] The differences in the Sm^+ cross section are observed in the apparent threshold that is ≈ 1 eV lower in energy for the ICP-MS/MS cross section than the GIBMS cross section;[15] nevertheless, the peak magnitude is very similar. Peak magnitude is also similar between ICP-MS/MS and GIBMS for Pr^+.[19] The overall cross section shape for the ICP-MS/MS U^+ reaction is different than the early ion beam experiment.[11] The early energy magnitude of the ion beam experiment is slightly higher in magnitude, though.

The differences here compared to the GIBMS experiments can likely be attributed (at least in part) to the starting electronic distribution. This is most evident in the shifted threshold or reaction (2) for Sm^+ that must indicate the presence of excited states. The Agilent instrument does not include a high pressure region (~ 500 mTorr) to collisionally cool reactants ions that the GIBMS[41] instrument does. Indeed, the SIFT-MS incorporates a similar high pressure drift tube.[7] Also, the present work was extrapolated to the single collision conditions where GIBMS naturally operates. Because the cross sections between the methods are within the combined uncertainties of those methods, this is probably an acceptable approach, but the cross section may retain some multi-collision character. In an ICP-MS/MS cross section of $Co^+ + O_2$ at higher pressures (3.5 mTorr), these pressure effects have appeared as increased cross section magnitude by a factor of 2 compared to GIBMS experiments.[31] Another potential difference is that the octopole only spans the physical length of the collision cell in the Agilent

instrument. Consequently, the effective cell length (from pumping gradients outside of the cell) will extend into regions pre and post octopole so that reactions or scattering outside of the collision cell may not be fully represented in the reaction cross section. Nevertheless, we anticipate that the relative trends from the work presented here are accurate.

Discussion

Previous work[39,42] has indicated that the bond dissociation energies (BDEs) of AnO^+ are correlated to the promotion energy of the first excited electronic state with two free 6d-electrons $[E_p(6d^2)]$. Similarly, Ln^+ BDEs have been correlated to the promotion energy to the first excited state with two free 5d-electrons $[E_p(5d^2)]$.[42] Armentrout[27] has recently shown that a better correlation exists between the BDEs and the excitation to Ln^{2+} $E_p(5d) + O^-$, but this argument only shifts how the electrons are shared within the bond and not the orbitals involved (*i.e.* two 5d-electrons are still needed to form the LnO^+ triple bond). Presumably this correlation exists because the four 2p-electrons in O can combine with the two free d-electrons to form a σ-bond and two π-bonds to form a robust triple bond. More recent work has also indicated a correlation of the rate of reaction (2) to $E_p(nd^2)$ for $n = 5$ and 6.[22] In this analysis, reaction efficiencies were taken from the SIFT-MS work of Bohme and coworkers[7] for the Ln^+ and the FTICR-MS work of Gibson and coworkers[1–3,5] for the An^+.

Fig. 3 presents a similar analysis from the current work for both the Ln^+ and An^+, indicating a strong linear correlation between the k/k_{col} and $E_p(nd^2)$. Noticeably, the cross sections of SmO^+ and EuO^+ in Fig. 1 show clear barriers. The result for EuO^+ is not surprising because this reaction is endothermic by 1.42 eV.[42] In the case of SmO^+, reaction (2) is exothermic by 0.143 eV, as
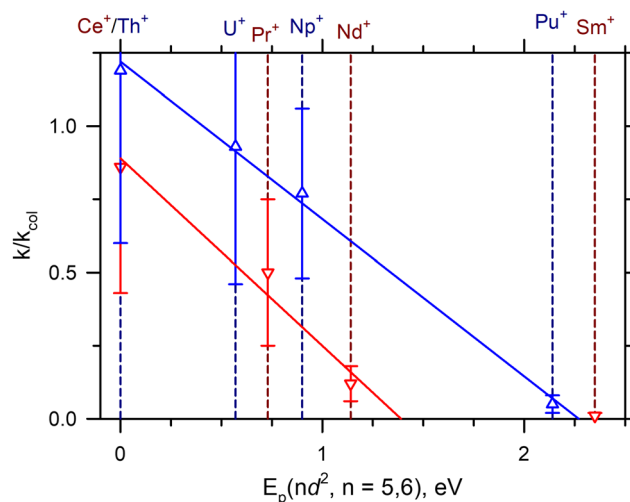

Fig. 3 Correlation of the reaction efficiency relative to the LGS collision rate (k/k_{col}) to the promotion energy $E_p(nd^2)$ for $n = 5$ (blue) and $n = 6$ (red). The solid blue and red line represent the least-squares linear regression fits of the Ln^+ and An^+ experimental data ($R^2 = 0.97$ and $R^2 = 0.99$). Sm^+ has been excluded from the Ln^+ linear regression fit. The dashed lines represent $E_p(nd^2)$ of the indicated cation with dark blue and dark red lines corresponding to Ln^+ and An^+ species, respectively. See also Table 1.

This journal is © the Owner Societies 2024

Phys. Chem. Chem. Phys., 2024, **26**, 209–218 | **213**

noted above. This barrier was observed previously in GIBMS experiments with carefully thermalized Sm^+ reactant ions.[15] *Ab initio* calculations indicate that this barrier could be attributed to the crossing seam between the potential energy surface (PES) of reaction (2) evolving from the ground state reactant asymptote and the PES evolving from an excited state reactant asymptote lying $E_p(5d^2)$ higher in energy, where the latter PES correlated with the formation of the SmO^+ ground state product. Here, similar barriers are also observed for PuO^+ and AmO^+ in Fig. 2, where reaction (2) is expected to be exothermic by 1.3 ± 0.2 eV and 0.35 ± 0.29 eV for Pu^+ ($D_0(Pu^+–O) = 6.75 \pm 0.20$ eV) and Am^+ ($D_0(Am^+–O) = 5.80 \pm 0.29$ eV),[39] respectively. As for Sm^+, the barriers observed for Pu^+ and Am^+ can may also be attributed to the energy at the crossing seam between the PESs evolving from the ground and reactive states. Interestingly, FTICR-MS reactions have indicated that for the much less thermodynamically favored reaction of Pu^+ with NO ($D_0(N–O) = 6.51$ eV),[36] $k/k_{col} = 0.17$ was observed, even though $\Delta H_r = -0.24 \pm 0.20$ eV is only mildly exothermic. Because the reaction of $M^+ + NO$ ($^2\Pi$) has less spin-restrictions than reaction (2), this observation may argue that spin conservation could still be important for heavy metals.

Reaction (2) requires that M^+ and MO^+ have the same spin state for the reaction to conserve spin. Table 3 lists the ground states of M^+ and the expected state of MO^+ from theoretical calculations and indicates that for the majority of M^+ in this study, the formation of ground state MO^+ from reaction (2) is indeed spin-forbidden. The exception is U^+ (^4I, $5f^37s^2$)[28] that likely forms UO^+ ($^4\Gamma$, $\pi\delta\phi$)[6] (where the orbital configuration listed is for the unpaired, non-bonding f-orbitals). Because the ground level of Th^+ is actually a mixed $^4F_{3/2}–^2D_{3/2}$ ($6d^27s/6d7s^2$)[43] configuration, reaction (2) forming ThO^+ ($^2\Sigma^+$, σ)[44] may also conceivably be considered spin-allowed. Given that reaction (2) is not spin-restricted for some of the An^+ but is for most, the strong correlation of reaction rate to $E_p(6d^2)$ in Fig. 3 suggests that $E_p(6d^2)$ has a stronger effect on the reaction rates than spin conservation.

Unlike the An^+, reaction (2) is likely formally spin-unallowed for the Ln^+ in this study, Table 3. There is a noticeable change in reaction efficiency between the Ln^+ and An^+, but many k/k_{col} are within the combined experimental uncertainties for each An^+ and Ln^+ congener of similar excitation energy, so it is also unlikely that spin-conservation plays a significant role at least at the lower energies. Like the An^+, the strong correlation of

$E_p(5d^2)$ to the rates of reaction (2) in Fig. 3 strongly suggests that $E_p(5d^2)$ more strongly influences the reaction rate than spin-conservation. Nevertheless, spin conservation may still play a role at higher energies.

A high energy feature is observed for CeO^+, PrO^+, and NdO^+ in Fig. 1 with apparent thresholds of ≈ 1–2.5 eV. Similar high energy features appear in the An^+ reactions, but these are less pronounced than those in the Ln^+ reactions. This feature was also observed in GIBMS studies of reaction (2) for Pr^+ and Nd^+, and it was speculated that this higher energy pathway was the formation of an excited state LnO^+ by a spin-allowed reaction. This was further substantiated by quantum chemical calculations that indicated at least one excited state with the correct spin and consistent excitation energy to the observed threshold.[17,19] These features appear inversely correlated with $E_p(nd^2)$; however, this is likely an artifact from the magnitude of the reaction cross section of the lower feature that obscures the start of the threshold region of the higher energy feature cross section. Indeed, when subtracting the low energy feature of the LnO^+ and AnO^+ cross sections in Fig. 1 and 2 by scaling the LGS cross section, the apparent thresholds are indistinguishable within the limits of uncertainty.

As noted above, it has been previously proposed that the role of $E_p(nd^2)$ in modulating the reaction rate is by partially determining the energy relative to the reactants of the crossing seam between the PESs originating from the ground state M^+ and the excited state with two d-electrons.[22] Here, we consider a simple potential energy surface that consists of an initial intermediate formed, an association of CO_2 with ground state M^+, forming the $M^+–CO_2$ adduct. This has been demonstrated for both Sm^+ and Gd^+, where $D_0(Sm^+–CO_2) = 0.42 \pm 0.03$ eV[15] and $D_0(Gd^+–CO_2) = 0.38 \pm 0.05$ eV[16] have been measured in collision induced dissociation (CID) reactions. A second intermediate presumably exists where the metal inserts into activated carbon dioxide bond forming $O–M^+–CO$. This is likely equivalent to an association complex between ground state MO^+ and CO. Indeed, CID reactions of such species yield $D_0(OSm^+–CO) = 0.97 \pm 0.09$ eV[15] and $D_0(OGd^+–CO) = 0.57 \pm 0.05$ eV[16] bond energies consistent with a weakly bound ion–dipole interaction. Thus, Table 3 indicates that $M^+–CO_2$ and $O–M^+–CO$ will usually have different spin states. Because formation of the MO^+ ground state requires two nd-electrons from M^+, the surface that includes the second intermediate

Table 3 Ground state reactants and products from reaction (2)[a]

Ln^+	Ce^+	Pr^+	Nd^+	Pm^+	Sm^+	Eu^+
$M^{+\,a}$	^4H ($4f5d^2$)	^5I ($4f^36s$)	^6I ($4f^46s$)	^7H ($4f^56s$)	^8F ($4f^66s$)	^9S ($4f^76s$)
MO^+	$^2\Phi$ (ϕ)[b]	^3H ($\delta\phi$)[c]	^4H ($\sigma\delta\phi$)[d]	$^5\Lambda$ ($4f^4$)[e]	$^6\Delta$ ($\phi^2\delta\pi^2$)[f]	$^7\Lambda$ ($4f^6$)[e]
An^+	Th^+	Pa^+	U^+	Np^+	Pu^+	Am^+
$M^{+\,bg}$	^4F–$^2D^h$ ($6d^27s/6d7s^2$)	^3H ($5f^27s^2$)	^4I ($5f^37s^2$)	^7L($5f^46d7s$)	^8F ($5f^67s$)	^9S ($5f^77s$)
$MO^{+\,i}$	$^2\Sigma^+$ (σ)[j]	$^3\Phi$ ($\sigma\phi$)	$^4\Gamma$ ($\pi\delta\phi$)	$^5\Gamma$ ($\sigma\pi\delta\phi$)	$^6\Sigma^+$ ($\sigma^2\phi^2$)n	$^7\Sigma^-$ ($\pi^2\delta^2\phi^2$)

[a] Ref. 28 (https://physics.nist.gov/PhysRefData/Handbook/periodictable.htm). [b] Ref. 26. [c] Ref. 19. [d] Ref. 17. [e] Presumed based on calculation trends. [f] Ref. 15. [g] Ref. 43 (https://www.lac.universite-paris-saclay.fr/Data/Database/). [h] See also ref. 13 and ESI. [i] Unless otherwise noted, ref. 6. [j] Ref. 44.

214 | *Phys. Chem. Chem. Phys.*, 2024, **26**, 209–218

This journal is © the Owner Societies 2024

must evolve from the excited state asymptote $E_p(nd^2)$ higher in energy than the ground state M^+. The MO^+ bond energy for An^+ and Ln^+ also depend upon $E_p(nd^2)$ because of the requirement of the two d-electrons to form the ground state bond so that the energy of the second intermediate is also partially set by this energy (the remaining influence is the strength of the OM^+–CO bond). The ground and excited state surfaces interact to form a crossing seam that must be traversed to form ground state products from the ground state reactants. Therefore, when $E_p(nd^2)$ is sufficiently high, as is the case for Sm^+, Eu^+, Pu^+, and Am^+, the barrier exceeds the reactants energy. When $E_p(nd^2)$ is sufficiently low, as is the case for Ce^+, Pr^+, Nd^+, Th^+, U^+, and Np^+ the barrier is localized between the two intermediates. Notably, the observed reaction rate is the equilibrium between the M^+–CO_2 falling apart forming the reactants and the forward reaction forming the products. Thus, the height of the crossing seam relative to the M^+–CO_2 adduct defines how competitive the forward reaction is compared to the backward reaction, and, therefore, the rate limiting step. Fig. 4 illustrates this concept using reaction (2) surfaces for U^+ and Pu^+. Fig. 4 is semiquantitative estimating intermediate well depths from Sm^+ CID reactions[15] and product energies from UO^+ and PuO^+ BDEs.[23,39]

The use of the Sm^+ data is likely reasonable assuming that the intermediates are only electrostatic interactions between the ground state reactant and the ground state product and the corresponding ligand (CO_2 and CO). However, there may be fundamental differences between Sm^+ and the An^+ that make this analysis, Fig. 4, semiquantitative. Most notably, f-orbital

participation cannot be ruled out with the present data. Nevertheless, there are key similarities between Sm^+ and Pu^+ that suggests that this explanation is plausible. Both Sm^+ and Pu^+ have similar promotion energies, $E_p(Sm^+)$ = 2.35 eV and $E_p(Pu^+)$ = 2.14 eV,[28] and both M^+ have barriers to an otherwise exothermic reaction as shown in Fig. 1 and 2. Computational modelling of the potential energy surface may provide additional information, but that is beyond the scope of this text.

The comparison of the Ln^+ and An^+ reaction (2) cross sections are also instructive. In general, the absolute magnitude of the AnO^+ cross sections are consistently higher than their Ln^+ counterparts. Because the primary difference between the Ln^+ and the An^+ is the possibility of the f-orbitals participating in the reaction, this difference may indicate 5f-orbital participation for the An^+. As noted above, the rate limiting step, the crossing seam energy, appears to be influenced by E_p and the insertion intermediate, O–M^+–CO. The interaction of the carbonyl with M^+ may indicate whether the 5f-orbitals participate in the O–An^+–CO through π^* back-bonding; however, CID reactions of $ThCO^+$ [$D_0(Th^+$–CO) = 0.94 ± 0.06 eV] indicate that even when back-bonding does occur,[21] it may not be sufficiently strong to distinguish between cases where it does not. Consequently, the carbonyl interaction is unlikely to greatly affect the energy of the crossing seam. The energy of the O–M^+–CO intermediate's energy is also set by the ground state product asymptote. Previous work has suggested an intrinsic BDE model[39,42] for both the LnO^+ and AnO^+. This model assumes that the orbitals used throughout both series to bind O are constant (*i.e.* the d-orbitals). Thus any LnO^+ or AnO^+ BDE could be calculated with knowledge of the intrinsic BDE [$D_0(M^+$–O)*] and the M^+ $E_p(nd^2)$ according to eqn (7):[42]

$$D_0(M^+-O) = D_0(M^+-O)^\star - E_p(nd^2) \tag{7}$$

Such a model suggests that the d-orbitals are primarily involved in forming the MO^+ bond. A careful comparison of the LnO^+ and AnO^+ BDEs trends suggests that the AnO^+ BDEs may include some 5f-orbital participation. This is observed by the slope of the LnO^+ trend *vs.* the slope of the AnO^+ trend in Fig. 5, where the latter deviates from the predicted slope (*i.e.* unity) in eqn (7). This suggests that 5f-orbital participation may be present in reaction (2) for the An^+. Notably, this is not an unambiguous indication of 5f-orbital participation. The AnO^+ BDEs in Fig. 5 are primarily from high temperature experiments extrapolated to 0 K, so the difference may only be experimental error. Likewise, other effects such as actinide contraction may explain some differences in observed trends. Nevertheless, the magnitudes of the AnO^+ cross sections compared to their Ln^+ congeners suggest some minor influence of the 5f-orbitals on the reaction rate.

Finally, Fig. 1 and 2 establish the presence of excited states in the current work when comparing the previous GIBMS work.[15,17,19] This is most notably evident in the threshold region of SmO^+, where the apparent threshold of the ICP-MS/MS work is approximately 1.5 eV lower in energy than the GIBMS work.[15] Excited states are expected in the current work because the ICP source temperature is 8000–10 000 K, and there is limited ability in the ICP-MS/MS to quench excited states
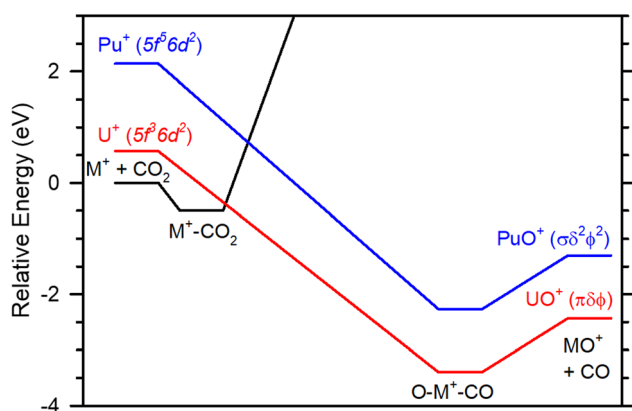

Fig. 4 Semiquantitative potential energy surface of $M^+ + CO_2 \rightarrow MO^+ +$ CO indicating that E_p and the intermediate well depth determine the crossing seam between the surface originating from the ground state reactant asymptote (black) and the surface leading to the ground state products. For species like Pu^+ (blue) that have a sufficiently high promotion energy, E_p = 2.14 eV,[39] the crossing between surfaces exceeds the reactant energy and a barrier is observed. For species like U^+ (blue) that have a lower promotion energy, E_p = 0.57 eV,[39] is lower than the reactant energy forming a localized barrier between the intermediates that affects the observed reaction efficiency. The intermediates are considered electrostatic interactions between ground state M^+ and CO_2 (M^+–CO_2) and ground state MO^+ and CO (O–M^+–CO). Values are estimated from Sm^+ CID reactions.[15] Product asymptotes are taken from the BDEs from Marcalo and Gibson[39] or Zhang *et al.*[23]
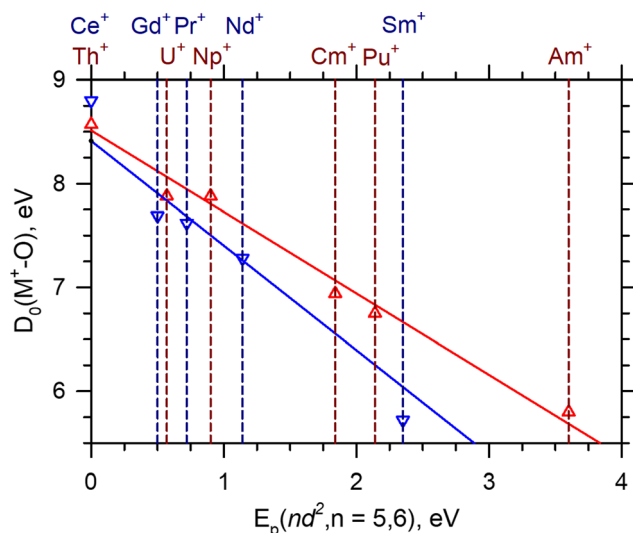
This journal is © the Owner Societies 2024

Phys. Chem. Chem. Phys., 2024, **26**, 209–218 | **215**

Fig. 5 LnO$^+$ (blue) and AnO$^+$ (red) BDEs as a function of $E_p(nd^2)$ for $n = 5$ and 6. Vertical dashed lines are $E_p(nd^2)$ for the indicated M$^+$. The solid lines represent the least-squares linear regression fit of each series. The LnO$^+$ fit is $8.41-1.01E_p(5d^2)$, $R^2 = 0.98$. The AnO$^+$ fit is $8.53-0.79E_p(6d^2)$, $R^2 = 0.98$. Ln$^+$ E_p and LnO$^+$ BDEs are taken from Gibson[42] or Armentrout and coworkers.[14,17,19,27,37] An$^+$ E_p and AnO$^+$ BDEs are taken from Marcalo and Gibson[39] or Armentrout and coworkers.[13,23] PaO$^+$ is not shown but included in the fit.

Conclusion

The energy dependence of the reactions of Ln$^+$ (Ln$^+$ = Ce$^+$, Pr$^+$, Nd$^+$, Sm$^+$ Eu$^+$) and An$^+$ (An$^+$ = Th$^+$, U$^+$–Am$^+$) with CO$_2$ were studied by ICP-MS/MS where the primary product observed was MO$^+$. k/k_{col}, compared to the LGS collision limit, for the barrierless exothermic reactions observed are correlated to $E_p(5d^2)$ for the Ln$^+$ and $E_p(6d^2)$ for the An$^+$ suggesting that the d-electrons are primarily involved in setting the rate of reaction (2). Barriers in excess of the reaction enthalpy were also observed for the reactions of Sm$^+$, Pu$^+$, and Am$^+$. These barriers can likely be attributed to a crossing seam between PESs originating from the ground state reactants and the excited state surface that leads to the ground state products. The energy of the crossing seam is likely determined by the energy of the reaction intermediates and E_p. For reaction (2), the energy of the more influential O–M$^+$–CO intermediate is heavily influenced by the product asymptote because it is a weakly bound complex between MO$^+$ and CO. Because the enthalpy of the reaction is also dependent on $E_p(nd^2)$, the promotion energy has a large impact so that even very exothermic reactions like Pu$^+$ + CO$_2$ ($\Delta H_2 = -1.30 \pm 0.20$ eV) may have a barrier if E_p (where $E_p(Pu^+) = 2.14$ eV[22]) is sufficiently high. This suggests that the nd-orbitals are primarily involved in reaction (2). Nevertheless, differences in the absolute reaction cross sections between the An$^+$ and Ln$^+$, where the former is generally greater than the latter, suggest that the 5f-orbitals play at least a minor role. This role is likely in forming the AnO$^+$ bond.

Notably, reaction (2), where CO$_2$ and CO are both singlets, is often spin-forbidden for M$^+$ all metals considered here except Th$^+$ and U$^+$. The correlation of the reaction rate to $E_p(nd^2)$ regardless of whether the reaction is spin-allowed indicate that for the Ln$^+$ and An$^+$, spin-restrictions do not appear to be a strong influence on the reaction rate.

prior to injection into the reaction cell. By contrast, the GIBMS work utilizes a 1 m tube pressurized to ≈ 0.5 Torr of buffer gas where ions undergo $\approx 10^5$ collisions.[41] A conservative estimate of the ion electronic distribution in the GIBMS experiments is 700 $\pm$ 400 K.[45–49] Likewise, the SIFT-MS experiments utilize a drift tube pressurized to 0.35 Torr with the reactive gas introduced downstream.[7] The Gibson and coworkers FTICR-MS work thermalized ions produced by laser desorption/ionization by cooling periods in 10^{-5} Torr Ar.[1–3,5] Notably, the FTICR-MS data is consistently low compared to GIBMS data. The difference is unclear. Nevertheless, GIBMS and SIFT-MS k/k_{col} for CO$_2$ are in good agreement, Table 2. This is likely due to similar thermalization processes of the ions prior to reaction that presumably yield similar electronic energy distributions. Assuming a 700 K distribution, the average electronic energy (E_{el}) is 0.00–0.06 eV, Table 1. By contrast, at 5000 K, E_{el} is 0.19–0.66 eV.

Excited states can, in principle, be more or less reactive than the ground state depending on how the PES evolves from that state. When many surfaces exist with crossing seams, then presumably a pathway exists for the reaction to proceed to product despite the contour of the starting PES. In this limit, E_{el} would act as additional energy for reaction. Because more energy is available for reaction, a more efficient reaction is observed. The Ln and An have many low-lying states,[28] so presumably the density of states in the reactant channel allows the extra E_{el} to act as additional energy available for reaction. Consequently, the higher electronic distribution in the ICP-MS/MS experiments likely leads to a higher observed reaction efficiency than the more thermalized GIBMS and SIFT-MS experiments, Table 2.

References

1 M. Santos, J. Marçalo, A. P. Matos, J. K. Gibson and R. G. Haire, Gas-Phase Oxidation Reactions of Neptunium

216 | *Phys. Chem. Chem. Phys.*, 2024, **26**, 209–218

This journal is © the Owner Societies 2024

and Plutonium Ions Investigated via Fourier Transform Ion Cyclotron Resonance Mass Spectrometry, *J. Phys. Chem. A*, 2002, **106**, 7190–7194.

2 M. Santos, J. Marçalo, J. P. Leal, A. P. Matos, J. K. Gibson and R. G. Haire, FTICR-MS Study of the Gas-phase Thermochemistry of Americium Oxides, *Int. J. Mass Spectrom.*, 2003, **228**, 457–465.

3 M. Santos, A. P. d Matos, J. Marcüalo, J. K. Gibson, R. G. Haire, R. Tyagi and R. M. Pitzer, Oxidation of Gas-Phase Protactinium Ions, Pa$^+$ and Pa^{2+}: Formation and Properties of PaO$_2$$^{2+}$(g), Protactinyl, *J. Phys. Chem. A*, 2006, **110**, 5751–5759.

4 J. K. Gibson, R. G. Haire, J. Marçalo, M. Santos, A. Pires de Matos, M. K. Mrozik, R. M. Pitzer and B. E. Bursten, Gas-Phase Reactions of Hydrocarbons with An$^+$ and AnO$^+$ (An = Th, Pa, U, Np, Pu, Am, Cm): The Active Role of 5f Electrons in Organoprotactinium Chemistry, *Organometallics*, 2007, **26**, 3947–3956.

5 J. K. Gibson, R. G. Haire, M. Santos, A. P. Matos and J. Marçalo, Gas-Phase Oxidation of Cm$^+$ and Cm^{2+} – Thermodynamics of Neutral and Ionized CmO, *J. Phys. Chem. A*, 2008, **112**, 11373–11381.

6 C. C. L. Pereira, C. J. Marsden, J. Marçalo and J. K. Gibson, Actinide sulfides in the gas phase: experimental and theoretical studies of the thermochemistry of AnS (An = Ac, Th, Pa, U, Np, Pu, Am and Cm), *Phys. Chem. Chem. Phys.*, 2011, **13**, 12940–12958.

7 P. Cheng, G. K. Koyanagi and D. K. Bohme, Gas-Phase Reactions of Atomic Lanthanide Cations with CO$_2$ and CS$_2$: Room-Temperature Kinetics and Periodicities in Reactivity, *J. Phys. Chem. A*, 2006, **110**, 12832–12838.

8 G. K. Koyanagi and D. K. Bohme, Oxidation Reactions of Lanthanide Cations with N$_2$O and O$_2$: Periodicities in Reactivity, *J. Phys. Chem. A*, 2001, **105**, 8964–8968.

9 P. Cheng, G. K. Koyanagi and D. K. Bohme, Gas-Phase Reactions of Atomic Lanthanide Cations with D$_2$O: Room-Temperature Kinetics and Periodicity in Reactivity, *ChemPhysChem*, 2006, **7**, 1813–1819.

10 R. M. Cox, P. B. Armentrout and W. A. de Jong, Activation of CH$_4$ by Th$^+$ as Studied by Guided Ion Beam Mass Spectrometry and Quantum Chemistry, *Inorg. Chem.*, 2015, **54**, 3584–3599.

11 P. B. Armentrout and J. L. Beauchamp, Reactions of U$^+$ and UO$^+$ with O$_2$, CO, CO$_2$, COS, CS$_2$ and D$_2$O, *Chem. Phys.*, 1980, **50**, 27–36.

12 R. M. Cox, J. Kim, P. B. Armentrout, J. Bartlett, R. A. VanGundy, M. C. Heaven, S. G. Ard, J. J. Melko, N. S. Shuman and A. A. Viggiano, Evaluation of the Exothermicity of the Chemi-ionization Reaction Sm + O → SmO$^+$ + e$^-$, *J. Chem. Phys.*, 2015, **142**, 134307.

13 R. M. Cox, M. Citir, P. B. Armentrout, S. R. Battey and K. A. Peterson, Bond Energies of ThO$^+$ and ThC$^+$: A Guided Ion Beam and Quantum Chemical Investigation of the Reactions of Thorium Cation with O$_2$ and CO, *J. Chem. Phys.*, 2016, **144**, 184309.

14 M. Demireva, J. Kim and P. B. Armentrout, Gadolinium (Gd) Oxide, Carbide, and Carbonyl Cation Bond Energies and Evaluation of the Gd + O → GdO$^+$ + e$^-$ Chemi-Ionization Reaction Enthalpy, *J. Phys. Chem. A*, 2016, **120**, 8550–8563.

15 P. B. Armentrout and R. M. Cox, Potential Energy Surface for Reaction of Sm$^+$ + CO$_2$ → SmO$^+$ + CO: Guided Ion Beam and Theoretical Studies, *Phys. Chem. Chem. Phys.*, 2017, **19**, 11075–11088.

16 M. Demireva and P. B. Armentrout, Activation of CO$_2$ by Gadolinium Cation (Gd$^+$): Energetics and Mechanism from Experiment and Theory, *Top. Catal.*, 2018, **61**, 3–19.

17 M. Ghiassee, J. Kim and P. B. Armentrout, Evaluation of the Exothermicity of the Chemi-ionization Reaction Nd + O → NdO$^+$ + e$^-$ and Neodymium Oxide, Carbide, Dioxide, and Carbonyl Cation Bond Energies, *J. Chem. Phys.*, 2019, **150**, 144309.

18 R. M. Cox and P. B. Armentrout, Activation of Water by Thorium Cation: A Guided Ion Beam and Quantum Chemical Study, *J. Am. Soc. Mass Spectrom.*, 2019, **30**, 1835–1849.

19 M. Ghiassee, B. C. Stevenson and P. B. Armentrout, Evaluation of the Pr + O → PrO$^+$ + e$^-$ Chemi-ionization Reaction Enthalpy and Praseodymium Oxide, Carbide, Dioxide, and Carbonyl Cation Bond Energies, *Phys. Chem. Chem. Phys.*, 2021, **23**, 2938–2952.

20 C. J. Owen, J. Kim and P. B. Armentrout, Holmium (Ho) Oxide, Carbide, and Dioxide Cation Bond Energies and Evaluation of the Ho + O → HoO$^+$ + e$^-$ Chemi-Ionization Reaction Enthalpy, *J. Chem. Phys.*, 2021, **155**, 094303.

21 A. Kafle, P. B. Armentrout, S. R. Battey and K. A. Peterson, Guided Ion Beam Studies of the Thorium Monocarbonyl Cation Bond Dissociation Energy and Theoretical Unveiling of Different Isomers of [Th,O,C]+ and Their Rearrangement Mechanism, *Inorg. Chem.*, 2021, **60**, 10426–10438.

22 R. M. Cox, K. Harouaka, M. Citir and P. B. Armentrout, Activation of CO$_2$ by Actinide Cations (Th$^+$, U$^+$, Pu$^+$, and Am$^+$) as Studied by Guided Ion Beam and Triple Quadrupole Mass Spectrometry., *Inorg. Chem.*, 2022, 8168–8181.

23 W. Zhang, A. R. E. Hunt, M. Demireva, J. Kim, K. A. Peterson and P. B. Armentrout, Bond Energies of UO$^+$ and UC$^+$: Guided Ion Beam and Quantum Chemical Studies of the Reactions of Uranium Cation with O$_2$ and CO, *Isr. J. Chem.*, 2023, e202300026.

24 M. Ghiassee, E. G. Christensen, T. Fenn and P. B. Armentrout, Guided Ion Beam Studies of the Dy + O → DyO+ + e- Chemi-ionization Reaction Thermochemistry and Dysprosium Oxide, Carbide, Sulfide, Dioxide, and Sulfoxide Cation Bond Energies, *J. Phys. Chem. A*, 2023, **127**, 169–180.

25 A. R. Bubas; W.-J. Zhang and P. B. Armentrout, 2023, work in progress.

26 T. Fenn; B. C. Stevenson and P. B. Armentrout, 2023, work in progress.

27 P. B. Armentrout, Periodic Trends in Gas-Phase Oxidation and Hydrogenation Reactions of Lanthanides and 5d Transition Metal Cations, *Mass Spectrom. Rev.*, 2022, 606–626.

28 J. E. Sansonetti and W. C. Martin. NIST Standard Reference Database 108. https://www.nist.gov/pml/handbook-basic-atomic-spectroscopic-data (accessed 03/02/2023).

29 J. O. Dimmock and A. J. Freeman, Band structure and magnetism of gadolinium metal, *Phys. Rev. Lett.*, 1964, **13**, 750.

This journal is © the Owner Societies 2024

Phys. Chem. Chem. Phys., 2024, **26**, 209–218 | 217

30 W. M. Temmerman; L. Petit; A. Svane; Z. Szotek; M. Lüders; P. Strange; J. B. Staunton; I. D. Hughes and B. L. Gyorffy, Chapter 241 The Dual, Localized or Band-Like, Character of the 4f-States, *Handbook on the Physics and Chemistry of Rare Earths*, Elsevier, 2009, vol. 39, pp. 1–112.

31 K. Harouaka, C. Allen, E. Bylaska, R. M. Cox, G. C. Eiden, M. L. Vacri, E. W. Hoppe and I. J. Arnquist, Gas-phase ion-molecule interactions in a collision reaction cell with triple quadrupole-inductively coupled plasma mass spectrometry: Investigations with N_2O as the reaction gas, *Spectrochim. Acta, Part B*, 2021, **186**, 106309.

32 P. B. Armentrout, Mass spectrometry – not just a structural tool: the use of guided ion beam tandem mass spectrometry to determine thermochemistry, *J. Am. Soc. Mass Spectrom.*, 2002, **13**, 419–434.

33 N. Yamada, Kinetic energy discrimination in collision/reaction cell ICP-MS: Theoretical review of principles and limitations, *Spectrochim. Acta, Part B*, 2015, **110**, 31–44.

34 G. Gioumousis and D. P. Stevenson, Reactions of Gaseous Molecule Ions with Gaseous Molecules. V. Theory, *J. Chem. Phys.*, 1958, **29**, 294–299.

35 E. W. Rothe and R. B. Bernstein, Collision Cross Sections for the Interaction of Atomic Beams of Alkali Metals with Gases, *J. Chem. Phys.*, 1959, **31**, 1619–1627.

36 NIST Computational Chemistry Comparison and Benchmark Database NIST Standard Reference Database Number 101 Release 16a. **https://cccbdb.nist.gov** (accessed 8/20/2014).

37 A. Lachowicz, E. H. Perez, N. S. Shuman, S. G. Ard, A. A. Viggiano, P. B. Armentrout, J. J. Goings, P. Sharma, X. Li and M. A. Johnson, Determination of the SmO^+ Bond Energy by Threshold Photodissociation of the Cryogenically Cooled Ion, *J. Chem. Phys.*, 2021, **155**, 174303.

38 H. H. Cornehl, R. Wesendrup, M. Diefenbach and H. Schwarz, A Comparative Study of Oxo-Ligand Effects in the Gas-Phase Chemistry of Atomic Lanthanide and Actinide Cations, *Chem. – Eur. J.*, 1997, **3**, 1083–1090.

39 J. Marçalo and J. K. Gibson, Gas-Phase Energetics of Actinide Oxides: An Assessment of Neutral and Cationic Monoxides and Dioxides from Thorium to Curium, *J. Phys. Chem. A*, 2009, **113**, 12599–12606.

40 R. M. Cox, A. Kafle, P. B. Armentrout and K. A. Peterson, Bond Energy of ThN^+: A Guided Ion Beam and Quantum Chemical Investigation of the Reactions of Thorium Cation with N_2 and NO, *J. Chem. Phys.*, 2019, **151**, 034304.

41 S. K. Loh, D. A. Hales, L. Lian and P. B. Armentrout, Collision-Induced Dissociation of Fe_n^+ (n = 2–10) with Xe: Ionic and Neutral Iron Cluster Binding Energies, *J. Chem. Phys.*, 1989, **90**, 5466–5485.

42 J. K. Gibson, Role of Atomic Electronics in f-Element Bond Formation: Bond Energies of Lanthanide and Actinide Oxide Molecules, *J. Phys. Chem. A*, 2003, **107**, 7891–7899.

43 J. Blaise and J.-F. Wyart, Energy Levels and Atomic Spectra of Actinides. **https://www.lac.universite-paris-saclay.fr/Data/Database/**(accessed 03/02/2023).

44 V. Goncharov and M. C. Heaven, Spectroscopy of the ground and low-lying excited states of ThO^+, *J. Chem. Phys.*, 2006, **124**, 064312.

45 C. L. Haynes and P. B. Armentrout, Thermochemistry and Structures of CoC3H6+: Metallacycle and Metal-Alkene Isomers, *Organometttalics*, 1994, **13**, 3480–3490.

46 D. E. Clemmer, Y.-M. Chen, F. A. Khan and P. B. Armentrout, State-Specific Reactions of $Fe^+(a^6D, a^4F)$ with D_2O and Reactions of FeO^+ with D_2, *J. Phys. Chem.*, 1994, **98**, 6522–6529.

47 B. L. Kickel and P. B. Armentrout, Guided Ion Beam Studies of the Reactions of Group 3 Metal Ions (Sc^+, Y^+, La^+, and Lu^+) with Silane. Electronic State Effects, Comparison to Reactions with Methane, and M^+-SiH_x (x = 0–3) Bond Energies, *J. Am. Chem. Soc.*, 1995, **117**, 4057–4070.

48 B. L. Kickel and P. B. Armentrout, Reactions of Fe^+, Co^+ and Ni^+ with Silane. Electronic State Effects, Comparison to Reactions with Methane, and M^+-SiH_x (x = 0–3) Bond Energies, *J. Am. Chem. Soc.*, 1995, **117**, 764–773.

49 M. R. Sievers, Y.-M. Chen, J. L. Elkind and P. B. Armentrout, Reactions of Y^+, Zr^+, Nb^+, and Mo^+ with H_2, HD, and D_2, *J. Phys. Chem.*, 1996, **100**, 54–62.

218 | *Phys. Chem. Chem. Phys.*, 2024, **26**, 209–218

This journal is © the Owner Societies 2024